ESD Investigations of Multiwalled Carbon Nanotubes

Mayank Shrivastava, *Member, IEEE*, Neha Kulshrestha, and Harald Gossner, *Senior Member, IEEE*

***Abstract*—Electrostatic discharge (ESD) investigations on the multiwalled carbon nanotubes (MWCNTs) are performed for the first time. A novel ESD failure mechanism of subsequent shell burning has been discovered. By using nanosecond pulse measurements, a new insight into metal-to-carbon nanotube (CNT) contact behavior could be achieved. Clear signature of two very different conduction mechanisms and related failure types at high current injection has been found. By determining the time to failure, an Arrhenius-like relation was extracted, which was explained by the oxidation of CNT shells. Finally, an extraordinary ESD failure current density of MWCNT of 1.2×10^9 A/cm^2 could be shown.**

***Index Terms*—Arrhenius behavior and graphene, carbon nanotubes, CNT, electrostatic discharge (ESD), high field transport, multiwalled carbon nanotubes (MWCNT), pulsed technique, quantum conductance.**

I. Introduction

In THE RECENT years, carbon based nano materials like Multiwalled Carbon nanotubes (MWCNT) have become one of the focus topic for beyond CMOS technologies [1], [2]. Conductance quantization, high field carrier transport, contact resistance and failure behavior of MWCNTs have been extensively studied for quasi-static operation [3], [15]. However, Electrostatic discharge (ESD) behavior of MWCNTs is still unknown. ESD is a fundamental reliability threat associated with semiconductor products, which occurs during handling, manufacturing and packaging of semiconductor chips. This requires rigorous device and circuit design measures. Often a new device or material needs to be investigated using transmission line pulse (TLP) tests, which in principle is nanosecond pulse (10 ns $\leq$ pulse-width $\leq$ 500 ns) I–V measurements. This work, for the first time, presents ESD/TLP behavior of MWCNTs.

Moreover, this work on MWCNTs, while using TLP for ns scale high current injection, also allows to study the carrier transport and failure behavior in more quantitative details and to separate between electrical and thermal phenomena. Most of the earlier investigations are based on quasi static or DC current-voltage measurements, which can lead to relevant joule heating [6] and optical phonon generation [7] (even at low bias[1]). This can conceal fundamental features of carrier transport and quantum conductance behavior. In this paper, investigations using ultra short (nanosecond scale) pulse I–V measurements will avoid these problems while allowing high current injection without leading to an early destruction.

The following phenomena have significantly impacted the electrical and failure behavior of CNTs:

(a) Quantized nature of conductance was detected and depicted in several works [3], [4]. Theories and experiments predict increased conductance with increase in tube's diameters [5].

(b) High field carrier transport in single wall CNTs (SWNTs) and MWCNTs has been widely studied [8]–[10]. Investigations in [8], [9] reported current saturation and fall in conductance of CNTs. Reference [8] found optical phonon scattering, zone boundary phonon scattering and phonon emission to be the dominating causes for current saturation. The saturated current was approximated by Landauer relation: $I_{\mathrm{SAT}} = (4e/h)\hbar\omega$, where I_{SAT} is the (measured) saturated current, h is Plank's constant and $\hbar\omega$ is the emitted phonon energy, which was back calculated to be equal to 0.16 eV. On the other hand, [9] claimed that the fall in conductance (or current saturation) was correlated with the decline in Density of States and number of the transverse modes available for transport at higher carrier energy. Contrary to aforementioned high field behavior, investigations in [10] found an improved conductance under high field condition, which was attributed to an onset of Zener tunneling across non-crossing subbands. Zener tunneling was indeed predicted to be the dominant mechanism of conductance larger than $4e^2/h$. Also, high field transport investigations are always limited due to early thermal destruction of tubes. Using extremely short pulses (with pulse widths on a nanosecond scale) for similar investigations can allow extremely high field carrier transport without a destruction of the tube.

(c) In the recent years, resistance of metal-carbon interface and its temperature dependency has been studied in detail [11]–[13]. In some works on graphene it was found

Manuscript received August 9, 2013; revised October 10, 2013; accepted October 18, 2013. Date of publication November 4, 2013; date of current version March 4, 2014.

M. Shrivastava is with the Department of Electronic Systems Engineering, Indian Institute of Science, Bangalore-560 012, India (e-mail: mayank@dese.iisc.ernet.in).

N. Kulshrestha was with the Department of Physics, Indian Institute of Technology Bombay, Mumbai-400 076, India. She is now with the Department of Photonics and Display Institute, National Chiao Tung University, Hsinchu 300, Taiwan.

H. Gossner is with the Mobile and Communications Group, Intel Corporation, 80336 Munich, Germany.

Color versions of one or more of the figures in this paper are available online at http://ieeexplore.ieee.org.

Digital Object Identifier 10.1109/TDMR.2013.2288362

[1]Low bias is a relative term, which depends on parameters like sample size/length, material's thermal properties and tube's diameter. For example temperature inside a 2 μm long and 5 nm wide (diameter) tube, while assuming 25 μA current through the tube at an applied bias of 0.5 V, can increase up to 500 K and 150 K for thermal conductivity of 300 W/K-m and 1000 W/K-m, respectively.

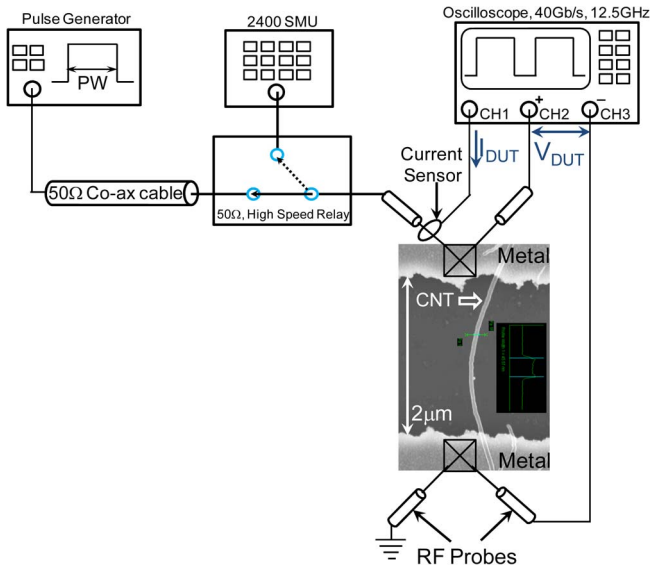

Fig. 1. Four probe measurement setup along with the SEM image of one of the MWCNT sample under test (DUT). A pulse generator capable of producing pulses with pulse width (PW) less than 1 ns up to few μs was used to stress the device. After each pulse measurement, a low bias DC test was performed to extract the change in tube's resistance (R). For this purpose, a high speed relay was used, which connects the SMU to the RF probes (contacting metal pads) after each pulse. Current and voltage waveforms were captured by a 40 Gb/s oscilloscope and were fed into a MATLAB program, which averages the data (80–90% of PW) and eventually produces one data point of the pulsed $I_{\rm DUT}-V_{\rm DUT}$ [Figs. 2(a)–4(a)].

that contact resistance decreases substantially as temperature increases [11], [12]. On the contrary, a recent work [13] found its opposite, i.e., substantial decrease of contact resistance by reducing temperature. This was attributed to reduced electron-phonon scattering at the metal-carbon interface at lower temperatures.

(d) Finally, most of the investigations dealing with failure behavior of CNTs assumed that carbon based material fails at $\sim$700 °C, when stressed in air [3], [4]. This was explained by onset of oxidation at 700 °C, which was later supported by higher failure threshold seen when CNTs where stressed in vacuum [15].

II. DUT and Experimental Setup

MWCNTs used in this work were grown by thermal CVD method using a mixture of ferrocene and toluene at a temperature of 850 °C. Grown tubes were then detached from the substrate and were individually dispersed on top of 250 nm thick metal (Cr/Au) pads on a Si/SiO_2 substrate. Spacing between individual metal pads was 2 μm (Fig. 1). Note that individual tubes are suspended between metal pads.

For electrical investigations, a very fast transmission line pulse (vf-tlp) setup was used, as shown in Fig. 1, capable of producing and capturing sub 5 ns of pulse width (PW). Four-probe vf-tlp, shown in Fig. 1, was used for pulse I–V measurements. For each voltage pulse (stress), current and voltage waveforms were captured by using a 12.5 GHz oscilloscope with 40 Gb/s of sampling rate. RF probes enable a short pulse (PW $\sim$5 ns, rise time $<$ 100 ps) measurements. By averaging over 70%–90% time window of the stress pulse waveform, a single data point

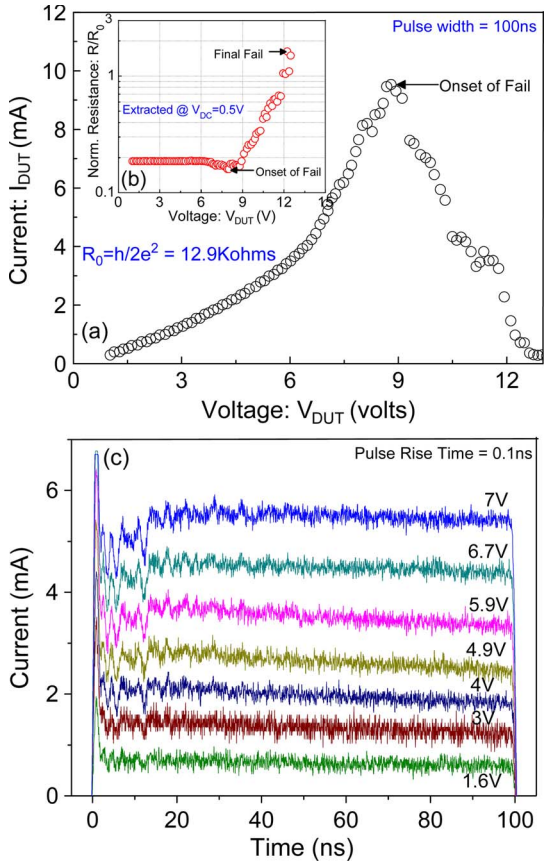

Fig. 2. (a) Pulsed (PW = 100 ns) $I_{\rm DUT}-V_{\rm DUT}$ characteristics of MWCNT sample-A, (b) tube resistance extracted at very low bias (0.5 V) after each pulse stress and (c) transient current waveforms as a function of time at different pulse voltages. $I_{\rm DUT}-V_{\rm DUT}$ relation shows only a single fail in the I–V characteristics and then subsequent fails occur almost close to the 1st failing voltage. Transient current waveforms show that current hardly changes with time.

of I–V characteristics is extracted. This was followed by a low bias DC test in order to find the change in MWCNT's resistance (R) after each pulse. This sequence was repeated for increasing voltage pulse amplitude.

In total 10 MWCNT samples were tested under vf-tlp stress conditions. 3 different types of I–V behaviors were identified and studied in-detail in next sections.

III. TLP Investigations

A. Unique TLP I–V Behaviors

Figs. 2(a)–4(a) show TLP $I_{\rm DUT}$–$V_{\rm DUT}$ characteristics of 3 different MWCNT samples. Sample-A [Fig. 2(a) and (b)] initially shows a linear I–V relation and an initial resistance of $0.2R_0(R_0 = h/2e^2)$. I–V behavior, however, changes as voltage across the tube increases beyond 6 V, and shows an exponential increase in current. The exponential increase in current may be attributed to onset of tunneling through non-crossing sub bands [10]. Finally, at higher stress (pulse) voltages, this MWCNT sample shows a gradual drop in current when $V_{\rm DUT}$ was increased beyond 9 V indicating a damage.

Unlike to sample-A, sample-B (Fig. 3) and sample-C (Fig. 4) initially show a linear $I_{\rm DUT}$–$V_{\rm DUT}$ relation until they depict

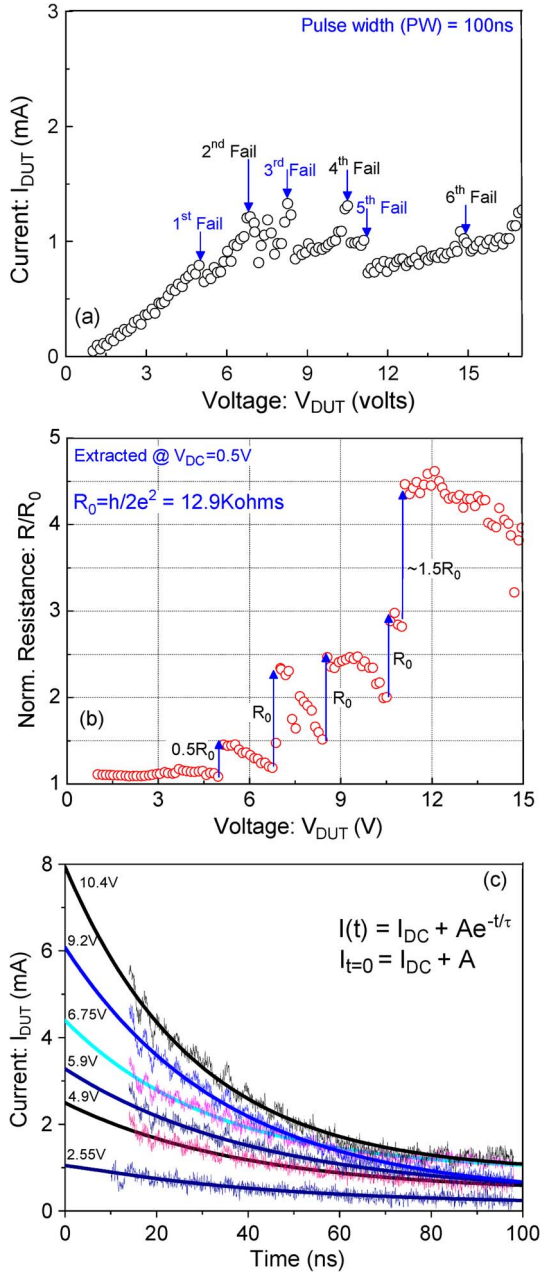

Fig. 3. (a) Pulsed (PW = 100 ns) $I_{\rm DUT}$–$V_{\rm DUT}$ characteristics of MWCNT sample-B, (b) tube's resistance extracted at very low bias (0.5 V) after each pulse stress and (c) transient current waveforms as a function of time at different pulse voltages. Current waveforms were nicely fitted (with less than 0.5% error) to an empirical relation: $I(t) = I_{\rm DC} + Ae^{-t/\tau}$, where $I_{\rm DC}$ is the DC current or current in steady state, A is the fitting constant and τ is the decay constant.

an abrupt drop in current when $V_{\rm DUT}$ was increased beyond 5 V and 6 V, respectively. There initial resistance was $\sim R_0$ and $0.5R_0$, respectively. An abrupt drop or change in current through multi walled nano tube (MWNT) at high bias is a well known signature of individual shell burning as reported in [15]–[17]. The interpretation is that a subsequent burning of single shells of the MWNT is observed until a complete open is reached. The behavior of sample-A is interpreted as simultaneous burning of all the CNT shells, leading to a single fail like signature in the I–V characteristics, after which tube's resistance gradually increases from $0.2R_0$ to beyond R_0.

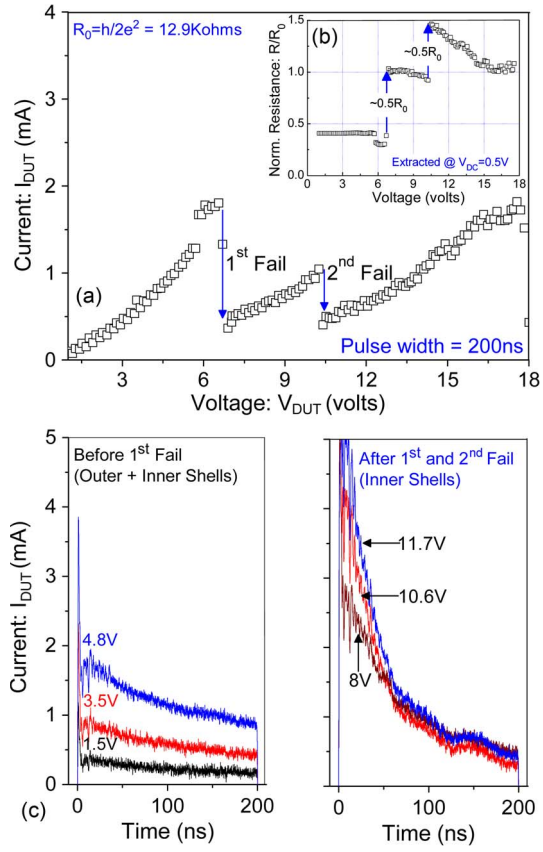

Fig. 4. (a) Pulsed I–V characteristics of MWCNT sample-C. (b) Normalized resistance extracted after each pulse. (c) Transient current waveforms as a function of time, which shows that current does not change over the time before the 1st fail; however, its behavior has changed after the 1st fail.

Whereas sample-B and sample-C have multiple fail (shell burning) signatures, each occurring at a pulse voltage higher than required for earlier fail. Note that (i) their respective resistances increase is quantized and is in steps of R_0 and $0.5R_0$, respectively, and (ii) jump in resistance and current drop, observed in the pulsed I–V characteristics, occur at the same time. This unique behavior and quantized change in resistance in steps of R_0 and $0.5R_0$ [Figs. 3(b) and 4(b)] after individual shell burning was not reported before. Equation (1) gives the expected/theoretical change in tube's resistance (ΔR) after individual shell burning, which was seen in most of the samples studied in this work

$$\Delta R = \frac{R_0}{n \cdot N \cdot (N-1)}; \qquad \text{where } R_0 = \left(\frac{h}{2e^2}\right) \tag{1}$$

where R_0 is the fundamental quantum resistance; n is number of conducting channels in a shell, which can be 1 or 2; N is number of conducting shells in a tube and h is Planck constant.

Figs. 3(a) and 4(a) also show increasingly higher voltage at same current for individual shell burning (current drop seen in $I_{\rm DUT}$–$V_{\rm DUT}$ characteristics), which is attributed to increased contact resistance after the burning of outer shells. Similar characteristics can also be seen in earlier works [16], [17], which used DC measurements. In [16] and [17] the difference between first fail and last fail (ΔV) is 0.4 V and 1.6 V, respectively. However, in this work a higher ΔV is observed, which ranges

TABLE I
OVERVIEW OF THE OBSERVED ELECTRICAL BEHAVIOR OF DIFFERENT CNT SAMPLES UNDER ESD TEST

Sample	Key Observations	Sample Type (Transient Response)
A (Fig. 2)	Tube's initial resistance: $0.2R_0$ Failure signature: Tube's resistance gradually increases from $0.2R_0$ to above R_0	Flat (Current does not change with time)
B (Fig. 3)	Tube's initial resistance: $\sim R_0$ Failure signature: Tube's resistance increases in steps of R_0 or $0.5R_0$	Exponentially Falling (Current falls exponentially with time)
C (Fig. 4)	Tube's initial resistance: $\sim 0.5R_0$ Failure signature: Tube's resistance increases in steps of $0.5R_0$	Crossover Behavior (Current remains unchanged with respect to time; however it falls exponentially after the first failure)

from 3 V to 10 V. The higher ΔV work is attributed to ESD time scale (nanosecond) pulse stress (10^5-10^6 times shorter compared to DC stress), which leads to higher failure voltage in order to satisfy energy-to-fail requirement.

B. Transient Behavior

Fig. 2(c) shows that current through the sample-A does not change over the stress time (*Flat Transient Response*), whereas the current through the sample-B falls exponentially with time [Fig. 3(c)] showing an *Exponential Falling Response*. Sample-C [Fig. 4(c)] shows a unique behavior where current transient is (initially) almost flat; however shows a *Crossover Behavior* as it falls exponentially after 1st fail. In Section IV, failure behavior of MWCNTs is discussed and linked with observed (i) *Flat Transient Response*, (ii) *Exponential Falling Response* and (iii) *Crossover Behavior*. Moreover, the respective transient behaviors are discussed in more detail in Section V. A summary of the observed behavior of various CNT samples, discussed in this section, is given in Table I.

IV. FAILURE ANALYSIS, JOULE HEATING AND ARRHENIUS RELATION

A. Failure Behavior and Analysis

It's widely reported that multiwalled carbon nanotubes, in contrast to metal wires, do not fail via electromigration. Instead, as depicted in [16], [17], MWCNT fails in a series of sharp steps associated with the destruction of individual nanotube shells. A similar behavior was observed in the ESD (nanosecond) time scale (Fig. 5); however the sharpness decreases, when the sample fails at shorter pulse times and becomes quite gradual in sub-100 ns time domain. This can be explained by partial loss of carbon when the CNT sample is stressed for very short times [18].

Post failure SEM pictures of MWCNT samples with an *Exponential Falling Response* have shown destruction always

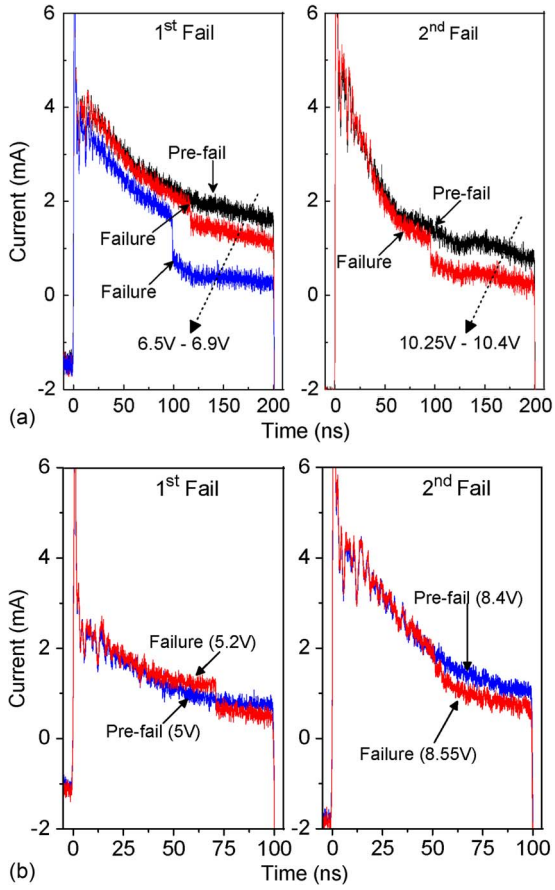

Fig. 5. Current waveforms depicting failure behavior under nanosecond scale stress. Figure (a) shows sharp step like fall associated with the destruction of individual nanotube shells, whereas (b) show that the sharpness decreases as time to failure reduces and become quite gradual in sub-100 ns time domain.

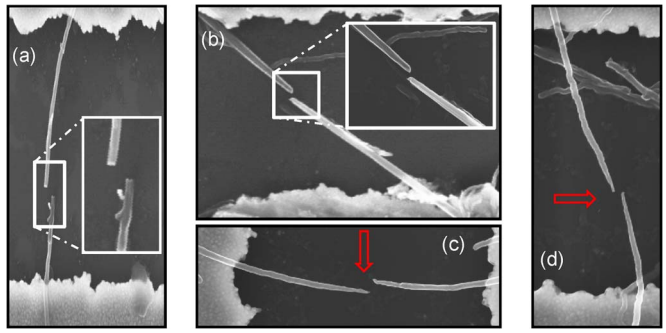

Fig. 6. Post failure SEM pictures of diffusive MWCNT samples stressed using pulses of different pulse widths (a): 10 ns, (b): 100 ns, (c): 200 ns and (d): 500 ns. In all the diffusive tubes the destruction was observed at the center. Interestingly, tube stressed by narrow/short pulse (a) breaks abruptly without any change in tube's diameter, whereas those destructed using longer stress pulse (b)–(d) has a higher loss of carbon.

at the center of the tube[2] (Fig. 6), while tube's destruction was seen always close to the metal contact[2] (Fig. 7) when transient current response was flat. Note that samples which failed close to metal contact were always found to have resistance lower

[2]Tubes which are failed close to metal contact have always shown transient behavior similar to the one shown in Fig. 2(c). However, tubes which failed at the center have always shown transient behavior similar to the one shown in Fig. 3(c).

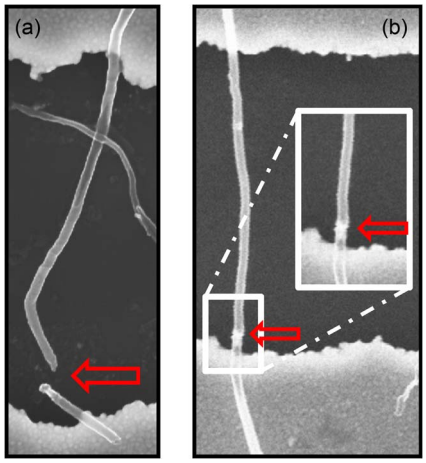

Fig. 7. Post failure SEM pictures of ballistic MWCNT samples. In all the ballistic tubes the destruction was observed close to the metal contact.

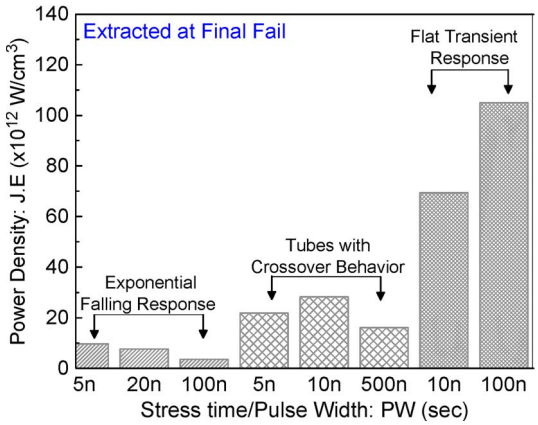

Fig. 8. Power density (J.E) extracted at the failure of individual samples (DUT). Figure shows that ballistic tubes fail at much higher power densities as compared to diffusive tubes. Note that x-axis shows the pulse width used for respective pulse I–V measurements.

$(< 0.5R_0)$ than those failed in the center $(> R_0)$. Hence, failure near contact must not be attributed to poor contacts unlike to report elsewhere [19].

Furthermore, tubes, with exponential falling response, stressed using narrow/short pulse [Fig. 6(a)] break abruptly without any major loss in carbon or change in tube's diameter close to failure site, whereas those destructed by longer stress pulse [Fig. 6(b)–(d)] show a higher loss of carbon around the failure site. Moreover, Figs. 6 and 7 depict that ESD time scale stress results into local burnout/shell removal, which is unlike to uniform shell removal reported in earlier works [16], [17]. This is attributed to localized hot spot resulted from nanosecond/ESD scale stress. However, in earlier works [16], [17] a steady state stress was used, which leads to a uniform temperature along the tube and results into uniform shell removal as soon as the outer shell reaches an appropriate temperature-to-burn (T_{BURN}).

B. Joule Heating, Power-to-Fail, and Contact Healing

Fig. 8 shows that tubes which were found to have flat current response as presented in Section III fail at much higher power densities when compared to tubes found have exponential

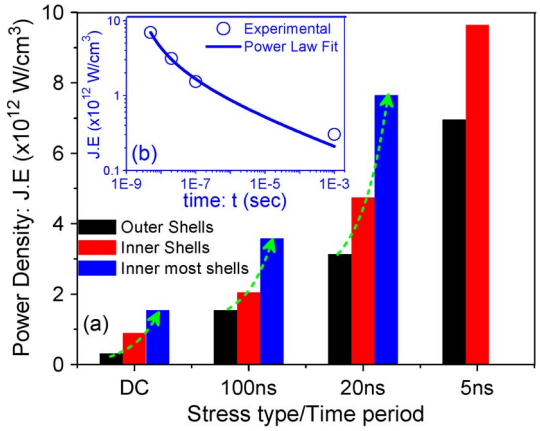

Fig. 9. (a) Power density (J.E) extracted at the failure of individual shells of different samples (DUT) showing diffusive transport, stressed using different pulse width. Figure shows that innermost shells fail at higher power densities as compared to outer shells. (b) Power law like behavior for tubes showing diffusive transport.

falling current response. This can be explained as follows: tubes showing an exponential falling current response are expected to have significant carrier scattering and therefore higher phonon energies. This will lead to lattice heating and eventual shell burning at lower power densities. On the other hand, samples with flat transient response, do not encounter significant electron-phonon scattering inside the tube. However, in these samples, scattering is expected to occur at the contacts, leading to a dissipation of energy at contacts. This would result into CNT-contact interface heating instead of direct heating of tube itself. Contacts are expected to be good heat sinks; still some heating will appear in the tube near the contacts. This can finally lead to shell burning close to the contact at high current and power density.

Fig. 9(a) shows power density required for failing inner and outer shells of CNT samples failed at the center of tube (i.e., with exponential falling response) and its relation with width of applied stress pulses. An increase of power-to-fail is observed from outer shells to inner shells. This can be attributed to an additional voltage drop at the contact after the burning of outer shells. Inset of Fig. 9 [(Fig. 9(b)] shows a power law like fitting of experimentally extracted power density (for outer shell/first fail). Measured data points fits well (less than 1% error) to the relation

$$\text{Power density (J.E)} = (a + bt^n)^{-1} \tag{2}$$

where fitting constants and exponent was found to be: $a = -5.8 \times 10^{-13}$ $\mathrm{W^{-1}cm^3}$, $b = 1.65 \times 10^{-11}$ $\mathrm{W^{-1}cm^3}$-sec and $n = 0.165$. The fitting depicts that the CNTs failing at the center of tube (possibly due to excess scattering) follow a power law like behavior $(y = b \cdot t^n)$ for shorter pulses; however, power-to-fail tends to saturate for longer pulses. This depicts that CNTs or other carbon based materials have a similar failure mechanism as that of metals and semiconductors.

Fig. 10 shows healing of contact resistance as the power density (J.E) inside the tube increases. This can be attributed to improved metal-carbon bonding at higher temperatures [20] resulted from Joule heating ($T \propto$ J.E).

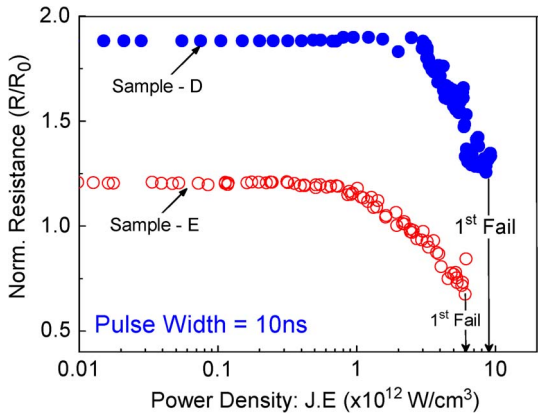

Fig. 10. Healing of contact resistance as the power density inside the tube increases. This can be attributed to improved metal-carbon bonding at higher temperatures resulted from joule heating. Note that the contact resistance improves systematically by increasing power density (i.e., lattice temperature).

C. Arrhenius Relation

Temperature at fail/burn $(T_{\rm BURN})$ was calculated by solving heat equation [eq. (3) and (4)]

$$\alpha \cdot \nabla^2 T + q = \frac{\partial T}{\partial t} \tag{3}$$

where $\alpha = \kappa/\rho \cdot C_p$ and $q = V_{\rm DUT} \cdot I_{\rm DUT}$

$$J \cdot E = \frac{4 \cdot I_{\rm DUT} \cdot V_{\rm DUT}}{\pi L d^2}. \tag{4}$$

Here, J is the current density in tube, E is the electric field across tube, $I_{\rm DUT}$ and $V_{\rm DUT}$ are current and voltage across tube, L and d are length and diameter of tube, respectively; T is lattice temperature, α is thermal diffusivity, κ is the thermal conductivity, ρ is mass density and C_p is the specific heat.

Calculated temperature was then fitted into an Arrhenius relation [eq. (5)] [21] where time-to-fail is indeed the width of applied stress pulse

$$k = Ae^{-E_a/RT}. \tag{5}$$

Here, k is the rate constant, A represents a pre- factor, E_a is the activation energy, R is the gas constant and T is temperature-to-fail/burn. Note that individual tubes are suspended on top of metal pads; therefore heat loss in substrate is ignored while solving the heat equation. Moreover, heat loss in metal contact is assumed to be minimal.

Fig. 11 shows that destruction of a nanotube in the nanosecond time range happens at much higher temperature ($\gg 700$ °C) than observed for DC stress. This is attributed to the fact that carbon shell/tube burning is a result of chemical process (reaction of carbon with oxygen in air), which is described by an activation energy (E_a).

A minimum value of the activation energy of 122 KJ/mol was reported in [21]; while the maximum value of 225 KJ/mol was extracted in [22]. Detailed investigations in [18] presented activation energy of 175 KJ/mol. The actual value depends on details of the material; it is higher for multiwalled CNTs or multi-layer graphene and lower for single walled CNTs and mono-layer graphene. The extracted value of E_a (Fig. 11) is 156 KJ/mol, which lies well in the reported range of 122 KJ/mol–225 KJ/mol [18], [21], [22].

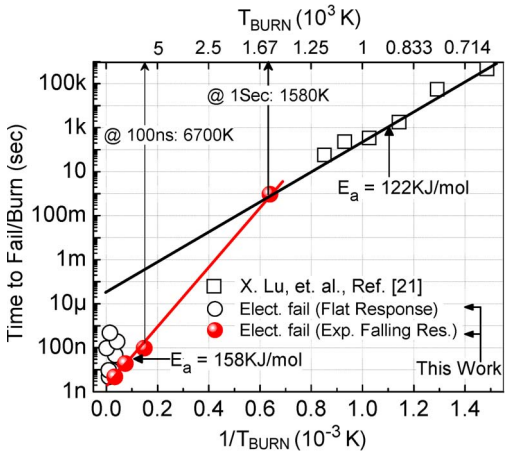

Fig. 11. Arrhenius plot extracted for nano tubes burned/failed under electrical stress in nanosecond time domain. (Temperature at fail was calculated by solving heat equation). Figure shows that the tubes require a much higher temperature ($\gg 700$ °C) in order to burn them in the nanosecond time range. Moreover, figure points that carbon shell/tube burning is chemical process driven by a required amount of energy (E_a).

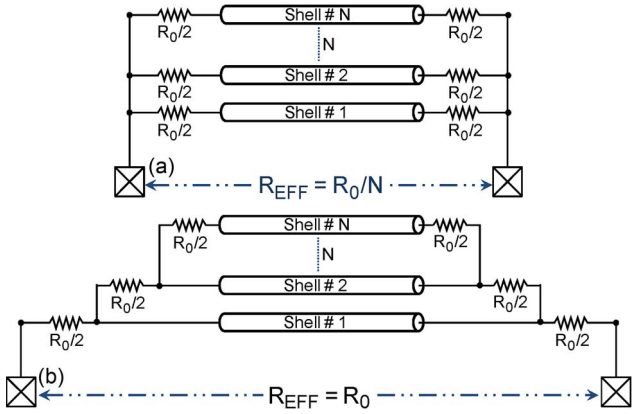

Fig. 12. Model depicting two unique ways by which individual shells of MWCNT couple with the contact/metal pad. (a), all (or most) of the shells with a resistance-to-contact equals to fundamental quantum resistance $(R_0 = h/2e^2)$ are in parallel to each other, resulting an effective tube resistance $(R_{\rm EFF})$ of R_0/N (N is the number of shells). (b), only the outermost shell (or few of the outermost shells) couples to the metal contact with a resistance close to R_0.

V. Carrier Transport and Relation With Quantum Resistance

A. Shell Coupling With Metal Contact

Change in resistance depicted in Figs. 2(b)–4(b) is used to model the coupling of individual shells of MWCNT with the contact/metal pad. Fig. 12 depicts two unique models: (a) all (or most) of the shells are parallel to each other where individual shells have a contact resistance equivalent to fundamental quantum resistance $R_0 = h/2e^2$ and (b) only the outermost shell connects directly to the metal contact with a contact resistance of R_0 and all inner shells (# m) couple to their respective outer shell (# m-1) only, with a resistance of R_0 between them. Two models result an effective tube resistance of R_0/N and R_0,

respectively, where the latter is independent of total number of shells. Change in resistance after individual shell burning can be calculated as $\Delta R = R_0/n \cdot N \cdot (N-1)$ and $\Delta R = R_0$, respectively for two models.

B. Ballistic and Diffusive Transport

As noted earlier, transient current waveforms [Figs. 2(c)–4(c)] show that current through the sample-A hardly changes over the stress time [Fig. 2(c)], whereas the same through the sample-B exponentially falls with time [Fig. 3(c)]. Sample-C shows a unique behavior where current transient is initially flat [Fig. 4(c)]; however it falls exponentially after 1st fail. As discussed earlier, the exponential fall[3] of current with time is attributed to a significant electron-phonon scattering leading to excess Joule heating in the sample-B and sample-C type MWCNTs. Joule heating substantially reduces the carrier scattering length as lattice temperature increases and eventually reduces the current through the tube. This behavior is qualitatively depicted in equations

$$R = \left(\frac{h}{2e^2}\right)\frac{L}{n \cdot N \cdot \lambda_{\text{eff}}} \tag{6}$$

$$\lambda_{\text{eff}} = \left(\lambda_{\text{AC}}^{-1} + \lambda_{\text{OP}}^{-1}\right)^{-1} \tag{7}$$

$$\lambda_{\text{eff}} = \frac{\lambda_{\text{eff}}(T = 300)}{T/300} \tag{8}$$

where λ_{eff} is the effective scattering length, λ_{AC} and λ_{OP} are the acoustic and optical phonon respective contributions, L is length of tube and T is lattice temperature. Such behavior is only possible in diffusive samples. In samples with flat transient behavior no self-heating seem to occur, which can indicate missing electron-phonon coupling in MWCNT e.g., by a ballistic transport.

For further analysis, current waveforms were fitted accurately to an exponential decay function [eq. (9)] and the decay rate/constant (τ) was extracted as a function of pulse voltage (Fig. 13)

$$I(t) = I_{\text{DC}} + Ae^{-t/\tau}. \tag{9}$$

Here, I_{DC} is the steady state or DC current, A is a fitting constant, t is time and τ is decay rate/constant.

The decay rate τ and its relation to applied voltage (V_{DUT}) can be used as an indicator for the nature of carrier and heat transport. High τ with no dependency on applied electric field (V_{DUT}/L) signifies ballistic transport, vice-versa for diffusive transport. Fig. 13 shows that sample-A has a very high τ, which initially did not show any dependence on pulse voltage (i.e., ballistic), whereas sample-B has an extremely low τ value and is inversely proportional to pulse voltage (i.e., diffusive). Furthermore, crossover (after 1st fail) from ballistic to diffusive can be seen in the sample-C [Fig. 13(c)]. Drop in τ value as pulse voltage/current increases is attributed to higher Joule heating inside the tube at increased J.E [eqs. (3) and (4)]. The different behaviors of individual MWCNTs presented in Fig. 13 and their respective change in resistance after individual shell burning depicts that the carrier transport in MWCNTs depends on the coupling of its conducting shells with metal contact.

[3]Note, that individual tubes in our work are suspended on metal pads. Since (i) there is no physical contact between CNTs and SiO2 and (ii) back gate of DUT is left floating, exponential fall of current with time cannot be attributed to charge trapping in SiO2. Moreover, charge trapping is typically not possible in 100 ns time scale [23].

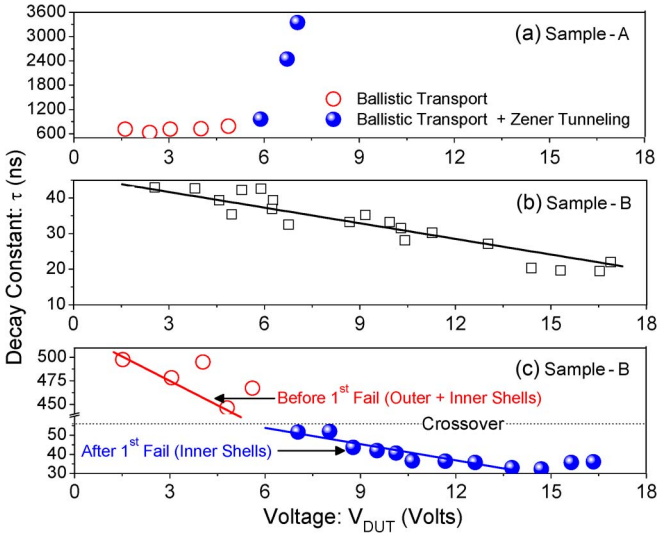

Fig. 13. Decay constant (τ) extracted for various tubes investigated. On one hand, sample-A has a high decay constant, which does not scale with increasing bias (or applied fields). This behavior depicts ballistic nature of sample-A. Moreover, decay constant of sample-A increases with increased Zener current, which further supports its ballistic nature. However, on the other hand, sample-B has a much lower decay constant compared to the sample-A, which drops linearly while increasing the pulse voltage (or applied field). This trend depicts diffusive nature and is attributed to reduced scattering length λ_{eff} resulting from a higher joule heating at higher J.E. A crossover from ballistic to diffusive transport was seen in sample-C as evident from very high decay constant before the 1st fail (depicting ballistic transport), which is reduced by $10\times$ after the 1st fail (depicting diffusive transport).

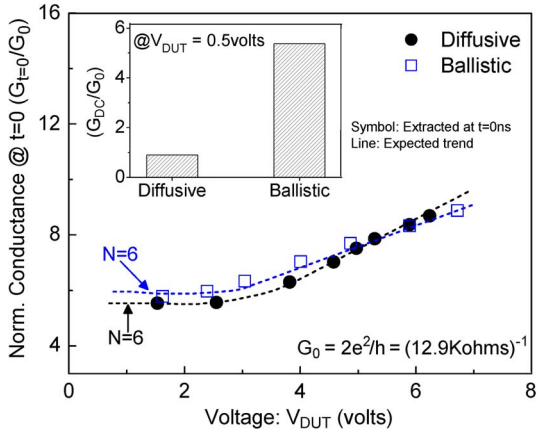

Fig. 14. Normalized conductance as a function of pulse voltage, extracted at $t = 0$ (time $= 0$) for different tubes. Inset compares their respective DC (steady state) conductance values at low bias. Extrapolation at $t = 0$, at which phonon energy cannot be higher than 25 meV (room temperature), excludes any contribution of optical phonons (160–200 meV), which can cause a significant scattering at the metal-CNT interface.

C. Considerations of Quantum Conductance and Relation With Optical phonons

Extrapolation of conductance (and current) at $t = 0$ (time $= 0$), is used to exclude Joule heating effects. Fig. 14 shows

TABLE II
ESD CURRENT DENSITY INSIDE TWO DIFFERENT MWCNT EXTRACTED AFTER A 100 ns TLP STRESS. NUMBER OF EXTRACTED SHELLS WAS 6 in BOTH THE TUBES (FIG. 14). FAILURE CURRENT DENSITY OF COPPER UNDER THE SAME STRESS WAS REPORTED TO BE 0.75×10^8 (A/cm^2) [24], [25]. S_{LAYER} $(= 3.4$ Å) IS THE SPACING BETWEEN TWO LAYERS

Sample type	External Diameter, d (nm)	Internal Diameter, ($d-2\cdot N\cdot S_{LAYER}$) (calculated using number of approximated shells)	Current, I_{FAIL} (mA) at the first fail (burning of outer shell)	Current density, J [$\times 10^8$(A/cm^2)] calculated using outer diameter: $J=\frac{4\cdot I_{FAIL}}{\pi\cdot d^2}$	Current density, J [$\times 10^8$ (A/cm^2)] calculated using outer & inner diameter: $J=\frac{I_{FAIL}}{\pi\cdot N\cdot S_{LAYER}\cdot(d-N\cdot S_{LAYER})}$
Ballistic	31.9	27.8	9.54	11.93	49.87
Diffusive	92.9	88.8	1.22	0.18	2.1

that avoiding Joule heating results in a much higher tube's conductance compared to the same extracted under quasi static condition (Inset: Fig. 14). This is attributed to a significantly lower carrier scattering at the metal-CNT interface when avoiding Joule heating and high phonon energy [13]. This difference was pronounced for diffusive tube as compared to ballistic, due to the fact that diffusive tubes have much higher Joule heating as compared to ballistic tubes. Moreover, conductance at $t = 0$ (and $V_{\mathrm{DUT}} = 0$ V) also gives a better estimate of number of conducting shells (N).

VI. ESD CURRENT DENSITY

ESD failure threshold (I_{FAIL}) of MWCNT, amounting to 9.5 mA for a tube with diameter ∼31.9 nm $(1.2 \times 10^9$ A/cm$^2)$, was found to be ∼16× higher than that of copper interconnects $(0.75 \times 10^8$ A/cm^2 [24], [25]). ESD behavior of CNT based interconnects depends on the nature of carrier transport in tube (Table II) and quality of CNT-to-metal contact. Ballistic tubes have higher I_{FAIL} compared to tubes with diffusive carrier transport. However, since ballistic or diffusive nature of CNTs depends on CNT-to-metal contact, I_{FAIL} values will eventually depend on the contact. For higher I_{FAIL} a good CNT-to-metal contact is therefore required.

VII. CONCLUSION

For the first time, TLP I–V and ESD failure investigations were performed for MWCNTs. A step-by-step destruction of individual shells with increasing pulse amplitude has been seen. The change in resistance after individual shell destruction was unique, showing a step-wise change in units of $h/2e^2$. This could be modeled by a simple resistive network representing the contact behavior. Different behavior of carrier transport in CNTs was detected by inspection of transient current waveforms and failure signatures. So-called "ballistic" tubes were identified in difference to "diffusive" tubes. The difference in behavior was found to be related to the varying contact resistance and the type of metal contact interface to carbon. It has been shown that diffusive tubes fail at much lower power densities compared to ballistic ones and that they follow a power law behavior. By solving heat equation, temperature at the destruction point of a shell was predicted, which is found to follow Arrhenius relation. This indicates that CNTs and probably even other carbon materials do not fail at a fixed temperature, but the failure progression is described by an activation energy. The importance of understanding the metal-to-carbon contact region has clearly been proven for CNTs under ESD conditions.

VIII. ACKNOWLEDGEMENT

N. Kulshrestha would like to acknowledge the Centre of Excellence in Nanoelectronics facilities at the Indian Institute of Technology Bombay, Mumbai, India.

REFERENCES

[1] H. Li, C. Xu, N. Srivastava, and K. Banerjee, "Carbon nanomaterials for next-generation interconnects and passives: Physics, status and prospects," *IEEE Trans. Electron Devices*, vol. 56, no. 9, pp. 1799–1821, Sep. 2009.
[2] N. Srivastava, H. Li, F. Kreupl, and K. Banerjee, "On the applicability of single-walled carbon nanotubes as VLSI interconnects," *IEEE Trans. Nanotechnol.*, vol. 8, no. 4, pp. 542–559, Jul. 2009.
[3] S. Frank, P. Poncharal, Z. L. Wang, and W. A. D. Heer, "Carbon nanotube quantum resistors," *Science*, vol. 280, no. 5370, pp. 1744–1746, Jun. 1998.
[4] A. Urbina, I. Echeverría, A. Pérez-Garrido, A. Díaz-Sánchez, and J. Abellán, "Quantum conductance steps in solutions of multiwalled carbon nanotubes," *Phys. Rev. Lett.*, vol. 90, no. 10, pp. 12–15, Mar. 2003.
[5] M. Liebau, E. Unger, F. Kreupl, A. P. Graham, G. S. Duesberg, and W. Steinhogl, "Carbon nanotubes in interconnect applications," *Microelectron. Eng.*, vol. 64, no. 1–4, pp. 399–408, Oct. 2002.
[6] K. H. Baloch, N. Voskanian, M. Bronsgeest, and J. Cumings, "Remote Joule heating by a carbon nanotube," *Nat. Nanotechnol.*, vol. 7, no. 5, pp. 316–319, May 2012.
[7] J. Y. Park, S. Rosenblatt, Y. Yaish, V. Sazonova, H. Üstünel, S. Braig, T. A. Arias, P. W. Brouwer, and P. L. McEuen, "Electron-phonon scattering in metallic single-walled carbon nanotubes," *Nano Lett.*, vol. 4, no. 3, pp. 517–520, Mar. 2004.
[8] Z. Yao, C. L. Kane, and C. Dekker, "High-field electrical transport in single-wall carbon nanotubes," *Phys. Rev. Lett.*, vol. 84, no. 13, pp. 2941–2944, Mar. 2000.
[9] Y. X. Liang, Q. H. Li, and T. H. Wang, "Current saturation in multiwalled carbon nanotubes by large bias," *Appl. Phys. Lett.*, vol. 84, no. 17, pp. 3379–3381, Apr. 2004.
[10] M. P. Anantram, "Current-carrying capacity of carbon nanotubes," *Phys. Rev. B, Condens. Matter*, vol. 62, no. 8, pp. 4837–4840, Aug. 2000.
[11] V. K. Nagareddy, I. P. Nikitina, D. K. Gaskill, J. L. Tedesco, R. L. Myers-Ward, C. R. Eddy, J. P. Goss, N. G. Wright, and A. B. Horsfall, "High temperature measurements of metal contacts on epitaxial graphene," *Appl. Phys. Lett.*, vol. 99, no. 7, p. 073506, Aug. 2011.
[12] Q. Shao, G. Liu, D. Teweldebrhan, and A. A. Balandin, "High-temperature quenching of electrical resistance in graphene interconnects," *Appl. Phys. Lett.*, vol. 92, no. 20, pp. 202108-1–202108-3, May 2008.
[13] F. Xia, V. Perebeinos, Y.-m. Lin, Y. Wu, and P. Avouris, "The origins and limits of metal–graphene junction resistance," *Nat. Nanotechnol.*, vol. 6, no. 3, pp. 179–184, Mar. 2011.
[14] B. Q. Wei, R. Vajtai, and P. M. Ajayan, "Reliability and current carrying capacity of carbon nanotubes," *Appl. Phys. Lett.*, vol. 79, no. 8, pp. 1172–1174, Aug. 2001.

[15] P. G. Collins, M. Hersam, M. Arnold, R. Martel, and P. Avouris, "Current saturation and electrical breakdown in multiwalled carbon nanotubes," *Phys. Rev. Lett.*, vol. 86, no. 14, pp. 3128–3131, Apr. 2001.
[16] P. G. Collins, M. S. Arnold, and P. Avouris, "Engineering carbon nanotubes and nanotube circuits using electrical breakdown," *Science*, vol. 292, no. 5517, pp. 706–709, Apr. 2001.
[17] B. Bourlon, D. C. Glattli, B. Placais, J. M. Berroir, C. Miko, L. Forro, and A. Bachtold, "Geometrical dependence of high-bias current in multiwalled carbon nanotubes," *Phys. Rev. Lett.*, vol. 92, no. 2, pp. 026804-1–026804-4, Jan. 2004.
[18] F. Stevens, L. A. Kolodny, and T. P. Beebe, Jr., "Kinetics of graphite oxidation: Monolayer and multilayer etch pits in HOPG studied by STM," *J. Phys. Chem. B*, vol. 102, no. 52, pp. 10 799–10 804, Dec. 1998.
[19] A. Liao, R. Alizadegan, Z.-Y. Ong, S. Dutta, F. Xiong, K. J. Hsia, and E. Pop, "Thermal dissipation and variability in electrical breakdown of carbon nanotube devices," *Phys. Rev. B, Condens. Matter*, vol. 82, no. 20, pp. 205406-1–205406-9, Nov. 2010.
[20] Q. Lv, M. X. Chen, H. Cao, and Z. Y. Gan, "An effective method for bonding carbon nanotubes onto metal electrodes," *Adv. Mater. Res.*, vol. 403–408, pp. 1099–1102, 2012.
[21] X. Lu, K. D. Ausman, R. D. Piner, and R. S. Ruoff, "Scanning electron microscopy study of carbon nanotubes heated at high temperatures in air," *J. Appl. Phys.*, vol. 86, no. 1, pp. 186–189, Jul. 1999.
[22] P. M. Ajayan, T. W. Ebbesen, T. Ichihashi, S. Iijima, K. Tanigaki, and H. Hiura, "Opening carbon nanotubes with oxygen and implications for filling," *Nature*, vol. 362, no. 6420, pp. 522–525, Apr. 1993.
[23] D. Estrada, S. Dutta, A. Liao, and E. Pop, "Reduction of hysteresis for carbon nanotube mobility measurements using pulsed characterization," *Nanotechnology*, vol. 21, no. 8, p. 085702, Feb. 2010.
[24] K. Banerjee, A. Amerasekera, and C. Hu, "Characterization of VLSI circuit interconnect heating and failure under ESD conditions," in *Proc. IEEE Int. Rel. Phys. Symp.*, 1996, pp. 237–245.
[25] S. Voldman, R. Gauthier, D. Reinhart, and K. Morrisseau, "High-current transmission line pulse characterization of aluminum and copper interconnects for advanced CMOS semiconductor technologies," in *Proc. IEEE Int. Rel. Phys. Symp.*, 1998, pp. 293–301.

Mayank Shrivastava (S'09–M'10) received the B.S. degree in engineering from Rajiv Gandhi Technical University, Bhopal, India, in 2006 and the Ph.D. degree from the Indian Institute of Technology Bombay (IIT), Mumbai, India, in 2010.

He has taken several positions within the semiconductor industry. During 2008 and again in 2010, he was a Visiting Scholar with Infineon Technologies AG, Munich, Germany. During 2010–2011, he was with Infineon Technologies, East Fishkill, NY, USA, and later with the Mobile and Communications Group, Intel Corporation, Hopewell Junction, NY. From October 2011 to August 2013, he was with the Mobile and Communications Group, Intel Corporation, Munich. Currently, he is an Assistant Professor with the Indian Institute of Science, Bangalore, India. He has more than 35 publications in international journals/conferences and has 18 U.S. patents issued or pending in his field of interest. His research interest includes advanced and beyond CMOS, on-chip electrostatic discharge (ESD) protection, device-circuit codesign, drain-extended MOS devices, and electrothermal modeling.

Dr. Shrivastava has served as a Reviewer for various international journals and in the Technical Program Committee of several international conferences, including EOSESD symposium in 2012, 2013, and 2014; IEEE ESSDERC 2014; IEEE VLSI 2014; and IEEE INDICON 2013. He was a recipient of the India TR35 Award in 2010 (Young Innovator Award from MIT Technology Review 35); the 2008 Best Research Paper Award in circuit design category from Intel Corporation Asia Academic Forum; the 2010 Industrial Impact Award from IIT Bombay; the biography publication by the International Biographical Center, Cambridge, U.K., in the 2000 Outstanding Intellectuals of the 21st Century in 2010; the Excellence in Thesis work for his Ph.D. thesis from IIT Bombay; and Infineon Ph.D. fellowship for three years.

Neha Kulshrestha was born in India in 1983. She received the B.Sc. and M.Sc. degrees from Dr. Bhim Rao Ambedkar University, Agra, India, in 2002 and 2004, respectively, and the Ph.D. degree in physics from the Indian Institute of Technology (IIT) Bombay, Mumbai, India, in 2013.

She was a Postdoctorate Fellow with the Department of Electrical Engineering, IIT Bombay, from April 2013 to October 2013. Currently, she is with the Department of Photonics and Display Institute, National Chiao Tung University, Hsinchu, Taiwan, as a Postdoctorate Fellow. Her research interests are the exploration of electrical properties of nanomaterials such as carbon nanotubes and graphene.

Dr. Kulshrestha was the recipient of 6th TSMC Outstanding Research Award 2012 (commendation) and the Malhotra Weikfield Foundation Nano Science Fellowship Award 2012 in the 5th Nano Bangalore Conference held in Bangalore, India.

Harald Gossner (M'06–SM'11) received the degree in physics (Dipl. Phys.) from Ludwig Maximilian University of Munich, Munich, Germany, in 1990 and the Ph.D. degree in electrical engineering from the Universität der Bundeswehr, Munich, in 1995.

He is a Senior Principal Engineer for electrostatic discharge (ESD) with Intel Corporation, Munich. For 15 years, he has worked on the development of ESD protection concepts for bipolar, BiCMOS, and CMOS technologies with Siemens and Infineon Technologies. Recently, he has joined the Mobile and Communications Group, Intel Corporation, where he oversees the development of robust mobile systems. He has authored and coauthored more than 80 technical papers and one book in the field of ESD and device physics. He holds 30 patents on the same topic.

Dr. Gossner is a member of ESDA and EDS. Regularly, he is lecturing tutorials at ESREF, IRPS, and EOSESD symposiums. He has served in the technical program committees of IEDM, EOSESD Symposium, and International ESD Workshop. He currently belongs to the management teams of IEW and EOSESD. In 2006, he became a Cofounder of the Industry Council on ESD Target Levels. Since then, he has been cochairing this committee of 50 leading electronics and IC companies. He was the recipient the best paper award of EOSESD 2005.